Nanoparticles

DOI: 10.1002/anie.201203581

Carbon-Coated Single-Crystal $LiMn_2O_4$ Nanoparticle Clusters as Cathode Material for High-Energy and High-Power Lithium-Ion Batteries**

*Sanghan Lee, Yonghyun Cho, Hyun-Kon Song, Kyu Tae Lee, and Jaephil Cho**

Lithium-ion batteries (LIBs) are expected to fulfill the rate capability and capacity requirements for a range of applications, from mobile devices to electric vehicles (EVs)/hybrid electric vehicles (HEVs) and even energy storage systems (ESSs). Conventional LIBs are unsuitable for applications with high-power requirements such as EVs and HEVs, as they exhibit low rate capability, especially during the charging process (that is, the batteries require a long time to charge). For EVs to become popular, battery charging should be completed in a few minutes, that is, in a comparable time to that required for filling automobiles with gasoline.

Recently, a spinel $LiMn_2O_4$ having a three-dimensional tunnel structure for the migration of lithium ions has received much attention as a potential high-power cathode material for LIBs because of its high operating voltage, abundance, low manufacturing cost, low toxicity, and excellent voltage profile compared to commonly used cathode materials such as layered $LiCoO_2$.[1] Moreover, $LiMn_2O_4$ has the advantage of fast charging because the delithiated structure of spinel $LiMn_2O_4$ is relatively stable in terms of thermodynamics and structure compared to that of layered materials such as $LiCoO_2$, which in an overcharged state undergo undesirable structural changes that degrade battery performance.[2] However, bulk $LiMn_2O_4$ did not fully satisfy high-power requirements because of their low electronic and ionic conductivities. On the other hand, it is well known that nanosized cathode materials offer higher rate capability by reducing lithium-ion-diffusion distances and increasing the contact area between the electrode and the electrolyte.[3] Therefore, in the past decade, the synthesis of nanostructured $LiMn_2O_4$ having various morphologies has been intensively studied to enhance the rate capability;[4] some notable results are summarized in Table S1 in the Supporting Information.

The disadvantage of nanosized materials is that they cannot be packed as densely on the current collector as micrometer-sized materials; this fact means that electrodes made of nanosized materials have a high porosity, thus resulting in a decrease the cell capacity. Therefore, the best way to improve both the rate capability and electrode density would be to use micrometer-sized particles that consist of aggregated nanoparticles.[5,6] The disadvantage of this arrangement, however, is that the primary particles located around the center of a nanocluster exhibit a large electric resistance because these particles are not connected with the conducting agent, thus resulting in a high overpotential during high-rate charging and discharging. To overcome this disadvantage, we hypothesized that the primary particles in spinel $LiMn_2O_4$ nanoclusters (Figure 1) could be coated with a thin carbon layer using sucrose as the carbon source. Sucrose carbonization on the single-crystal particle surface resulted in the formation of an electrical network within the secondary particle (Figure 1b). The use of this proposed material in a cell afforded not only an extremely high rate capability but also a high energy density. The material exhibits a gravimetric energy of 300 Wh per kg of active material (kg_{am}) while delivering a power of 45 kW/kg_{am} and a volumetric energy of 440 Wh per liter of electrode (L_e) while delivering 68 kW/L_e of power. The use of this material would enable the lithium-ion battery to be charged up to 97% in

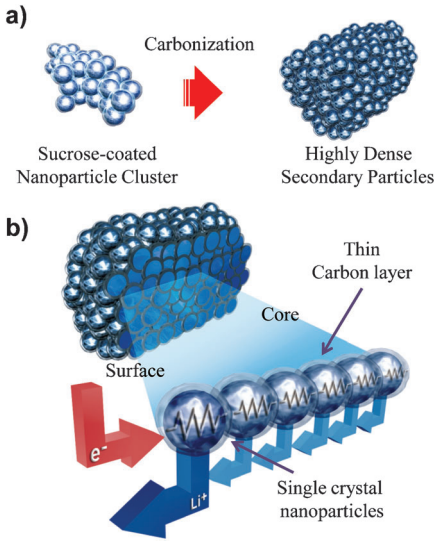

Figure 1. Fabrication process and electrical circuit configuration of carbon-coated single-nanoparticle clusters. a) The carbon coating of single-crystal nanoparticles was achieved by sucrose carbonization in air. b) Cross-section and electric-circuit configuration in a nanoparticle cluster. A single-crystal of $LiMn_2O_4$ is covered with a thin carbon layer that forms an electrical network in the nanoparticle cluster.

[*] S. Lee, Y. Cho, Prof. H. K. Song, Prof. K. T. Lee, Prof. J. Cho
Interdisciplinary School of Green Energy
Ulsan National Institute of Science and Technology (UNIST)
Ulsan, 689-798 (South Korea)
E-mail: jpcho@unist.ac.kr
Homepage: http://www.jpcho.com

[**] This research was supported by the Converging Research Center Program through the Ministry of Education, Science and Technology (2012K001251).

Supporting information for this article is available on the WWW under http://dx.doi.org/10.1002/anie.201203581.

100 s and deliver over 63% of the initial capacity after 2000 cycles without changing power, at the same charge and discharge rates of 20 C (≈3 min).

$LiMn_2O_4$ nanoparticles of size 20 nm (see the Supporting Information, Figure S1) were hydrothermally prepared from a mixture of lithium hydroxide, manganese acetate, and hydrogen peroxide heated at 110 °C for 12 h; this temperature is lower than those reported in literature.[7] The solvent dependence of the morphology (Figure S2) was also investigated, and methanol-assisted solubilization products showed regular-shaped nanoparticles with a narrow size distribution. Such particles can be easily packed to attain a relatively high electrode density (Figure 2a).[8] These particles were then used to fabricate the two active materials evaluated in this study: 1) carbon-coated single-crystal $LiMn_2O_4$ nanoparticle clusters (CSC-NPs) and 2) quenched single-crystal $LiMn_2O_4$ nanoparticle clusters (QSC-NPs). Additionally, 3) polycrystalline $LiMn_2O_4$ microparticles (PC-MPs) were prepared by solid-state reaction so for investigations into the effect of the size of the particles.

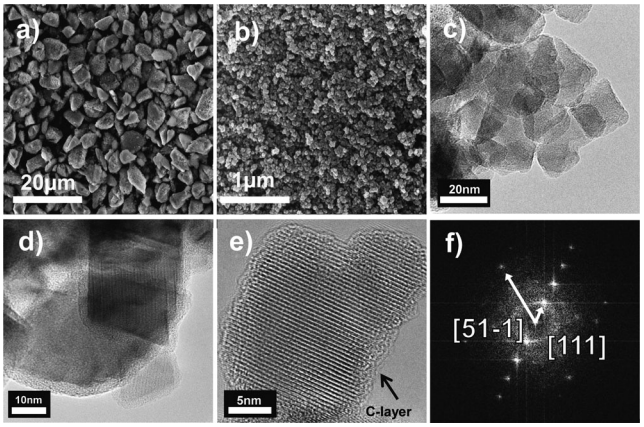

Figure 2. Characterization of carbon-coated single-crystal $LiMn_2O_4$ nanoparticle clusters (CSC-NPs). a, b) SEM images showed highly aggregated nanoparticle clusters. Scale bars: 20 μm (a), 1 μm (b). c, d, e) HRTEM images of CSC-NPs showed single-crystal nanoparticles that were 20 nm in size, and a thin carbon layer on the single-crystal nanoparticle. Scale bars: 20 nm (c), 10 nm (d), 5 nm (e). f) Fast Fourier transform images of e).

The fabrication of CSC-NPs involved coating the particles with a thin carbon layer by mixing as-prepared $LiMn_2O_4$ nanoparticles (NPs) with sucrose and quenching at 600 °C for 10 min. The resulting nanoparticles showed a highly aggregated morphology (Figure 2a and b) with a pellet density of greater that 2.6 $g\,cm^{-3}$, and the carbon layer was found to be evenly distributed (Figure 2d,e; Supporting Information Figures S3 and S4). The carbon content was 0.15 wt.%, as obtained using an element analyzer. Fast Fourier transform (FFT) images of single particles before coating and after coating showed the same diffraction pattern along the [−110] zone axis (see the Supporting Information, Figures S3c and S3d). Moreover, the XRD patterns and particle size (Table 1) of these samples did not change. This finding indicates that carbon coating does not affect the structure and particle size of $LiMn_2O_4$ nanoparticles. QSC-NPs were fabricated in the same manner as the CSC-NPs, but without sucrose. XRD patterns of three samples are shown in the Supporting Information Figure S5a. PC-MPs were prepared by a solid-state reaction. All the diffraction patterns of the samples can be assigned to the cubic spinel phase ($Fd\bar{3}m$) and correspond well to JCPDS data (35-0782) without any impurity phases. The lattice parameter, particle size, surface area, and pellet density of the samples are summarized in Table 1.

Table 1: Characterization of carbon-coated single-crystal $LiMn_2O_4$ nanoparticle cluster (CSC-NPs) and control group (QSC-NPs and PC-MPs).

Sample (Control group)	Empirical formula	Surface area [$m^2\,g^{-1}$]	Average particle size	Lattice parameter [Å]	Pellet density [g/CC]
CSC-NPs	$Li_{1.02}Mn_{1.98}O_4$	67.0	>20 nm	8.2223(6)	2.6
QSC-NPs	$Li_{1.02}Mn_{1.98}O_4$	65.0	>20 nm	8.2264(4)	2.6
PC-MPs	$Li_{1.01}Mn_{1.99}O_4$	0.4	13 μm (D50)	8.2421(3)	2.9

The electrochemical performance of CSC-NPs was evaluated (Figure 3 and Supporting Information Figure S6) in pouch-type half cells having an area of 2 cm × 1 cm. All cells were fabricated identically and initially cycled at 0.1 C and the first discharge capacities of the CSC-NPS, QSC-NPs, and PC-MPs were 120 $mA\,h\,g^{-1}$, 120 $mA\,h\,g^{-1}$, and 105 $mA\,h\,g^{-1}$, respectively, with a coulombic efficiency of 96%, 96%, and 98%, respectively. Coulombic efficiencies of the samples were greater than 99.9% for the rest of cycles. To investigate the charge rate capability, the cells were charged galvanostatically to 4.5 V at various rates ranging from 0.5 C to 100 C and then discharged at 1 C (Figure 3a, and Figure S6a in the Supporting Information). CSC-NPs and QSC-NPs exhibited a first discharge capacity of 120 $mA\,h\,g^{-1}$ after 0.5 C charging. Compared with practical capacity at 0.5 C, the CSC-NPs retained 95.3% capacity at 10 C (343 s) and 83.1% at 50 C (59 s), whereas the QSC-NPs retained 84% at 10 C and less than 5% capacity at 50 C. These results imply that CSC-NPs can be charged to 95.3% in 6 min and 83.1% in 1 min by the constant current mode. The discharge rate performance was also investigated by setting the charge rate as 0.5 C and increasing the discharge rate from 1 C to 300 C (Figure 3b, and Figure S6b in the Supporting Information). The PC-MP electrode showed higher rate performance than commercial LIBs because of their low electrode-loading levels and higher content of conducting agent. However, the CSC-NPs retained 89% (64 s), 84% (30 s), and 47% (6 s) of the initial capacity at 1 C at discharge rates of 50, 100, and 300 C, respectively. Figure 3c and Figure S6c, in the Supporting Information, show the discharge capacity as a function of the cycle number with increasing C rate, from 1 C to 100 C, between 3 and 4.5 V (same charge and discharge rates were used). The CSC-NPs exhibited discharge capacities of 121 $mA\,h\,g^{-1}$, 108 $mA\,h\,g^{-1}$, and 80 $mA\,h\,g^{-1}$ at rates of 1 C, 50 C, and 100 C, respectively (1 C = 120 $mA\,g^{-1}$). Therefore, a cycle at 100 C takes only 48 s with the cell retaining 66% of its initial capacity. Figure 2c was converted into a Ragone plot (Figure 3d and e). Remarkably, the CSC-NPs exhibited a gravimetric energy of

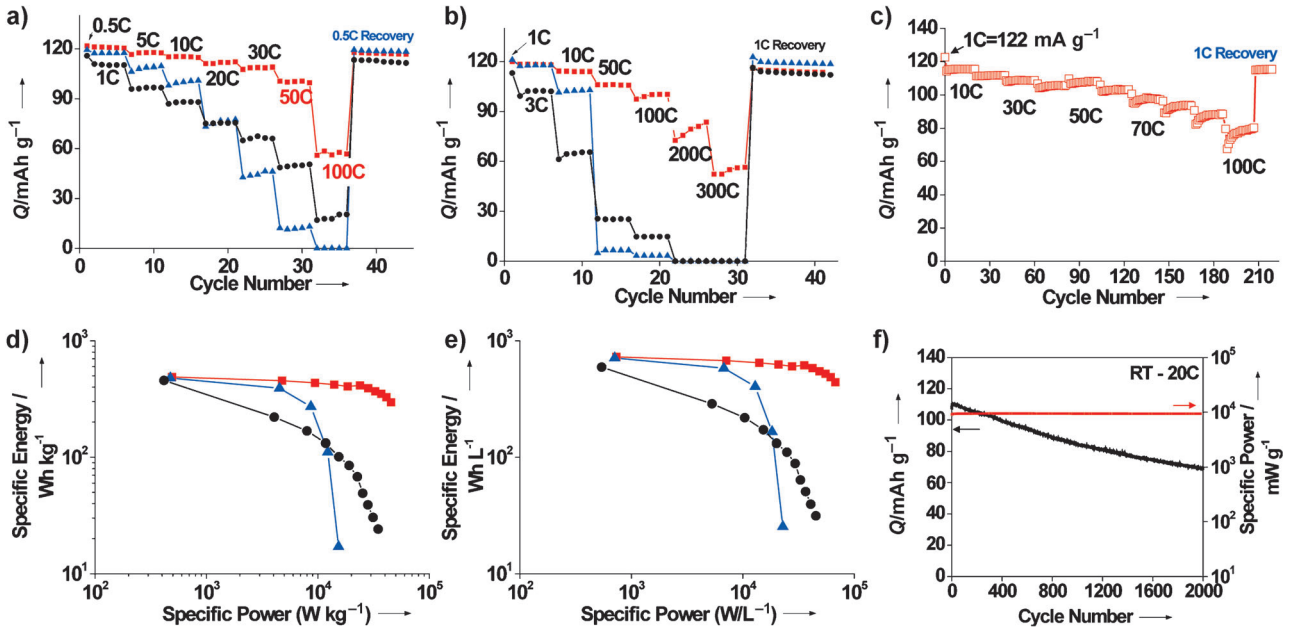

Figure 3. Charge and discharge rate capabilities for CSC-NPs (red square), QSC-NPs (blue triangle), and PC-MPs (black circle) tested between 3.0 and 4.5 V. a) 1 C discharge capacities (Q) after different charge rates versus cycle number. b) Discharge capacity versus cycle number under different C rates (1–300 C). The cell was charged at 0.5 C, and then discharged at different C rates. High rate cycle performance of CSC-NPs is shown in c). c) Discharge capacity versus cycle number with C rate increasing from 1 C to 100 C. Cycles were repeated 20 times for each of the rates (the same charge and discharge rates were used). d and e) Ragone plot showing higher power performance of CSC-NPs compared to QSC-NPs and PC-MPs (gravimetric energy: 300 Wh kg_{am}^{-1} while delivering 45 kW kg_{am}^{-1} power; volumetric energy: 440 Wh L_e^{-1} while delivering 68 kW L_e^{-1}. The weight used for the volume calculation included the weight of only the active material and electrodes (without current collector). The electrode-loading level, density, and thickness of CSC-NPs and QSC-NPS electrode were 3.6 mg cm^{-2}, 2.3 g cm^{-3}, and 16 μm, and those of PC-MPs electrode were 3.0 mg cm^{-2}, 2.0 g cm^{-3}, and 15 μm, respectively. f) Black line shows cyclabililty at 20 C; red line shows that specific power can be maintained without any evidence of decay for over 2000 cycles. Voltage profiles of a), b), c), and d) are described in the Supporting Information (Figure S6).

300 Wh/kg_{am} while delivering a power of 45 kW/kg_{am} and a volumetric energy of 440 Wh/L_e while delivering a power of 68 kW/L_e. In comparison with previous studies[4c–g,8] shown in Table S1, the CSC-NP electrode shows far superior performances with respect to the electrode loading levels, densities, and thicknesses.[4,9] To investigate cycle retention at high rates, these materials were cycled at a rate of 20 C for 2000 cycles (Figure 3 f, and Figure S6d in the Supporting Information). The specific power of a 20 C cycle of an LIB is comparable with that of variable capacitors.[10] With an initial capacity of 110 mA h g^{-1}, 90 % of the initial capacity was maintained even after 400 cycles. Even after 2000 cycles, capacity retention was 63 % and more importantly, the specific power did not change for different number of cycles because the average voltage was almost constant with respect to the number of cycles (Figure S6d in the Supporting Information). In addition, a stepwise charging method was used for boosting charge (Figure S7 in the Supporting Information). This charging method can allow the CSC-NP electrode to be charged to 98 % of 1 C capacity in 100 s, and 90 % of its initial capacity was delivered after 200 cycles.

To investigate the nanosize effect and the role of the thin carbon-layer coated on the primary particles, electrochemical impedance spectroscopy was performed. According to the random-walk theory, the relaxation time is given by $\tau = r^2/6D$ (three-dimensional diffusion), and lithium-ion diffusion in active materials is considered as the slowest diffusion in lithium-ion battery systems.[11] If the rate capability of these battery systems was controlled by lithium-ion diffusion in active materials, then 20 nm active materials, which have a diffusion coefficient of 10^{-12} to 10^{-6} cm^2s^{-1}, would be fully discharged or charged in 0.1 ns to 0.1 ms, respectively. Therefore, the electron delivery to the active materials or the charge-transfer reaction on the interface between the active materials and the electrolyte must be the rate-limiting factor for fast charge and discharge. Using the Arrhenius equation, the activation energies (E_a) for the reaction on a particle surface could be calculated from the temperature dependencies (Figure 4 a) of charge-transfer resistances (R_{ct}), which are shown by semicircles in middle frequency (Figure 4 b and S8). The activation energies of CSC-NPs, QSC-NPs, and PC-MPs for charge transfer were 0.46 eV, 0.43 eV, and 0.54 eV, respectively. Maier and co-workers reported that for particles smaller than 100 nm, electrochemical properties were affected by surface energy,[12] and therefore, it is concluded that the charge-transfer reaction of CSC-NPs and QSC-NPs is accelerated as a result of this size effect, thus giving rise to a higher rate performance. However, CSC-NPs showed a much higher rate performance than QSC-NPs despite the higher activation energy of the former. The galvanostatic intermittent titration technique (GITT) (Figure 4c,d and S9) showed different potential responses of CSC-NPs and QSC-

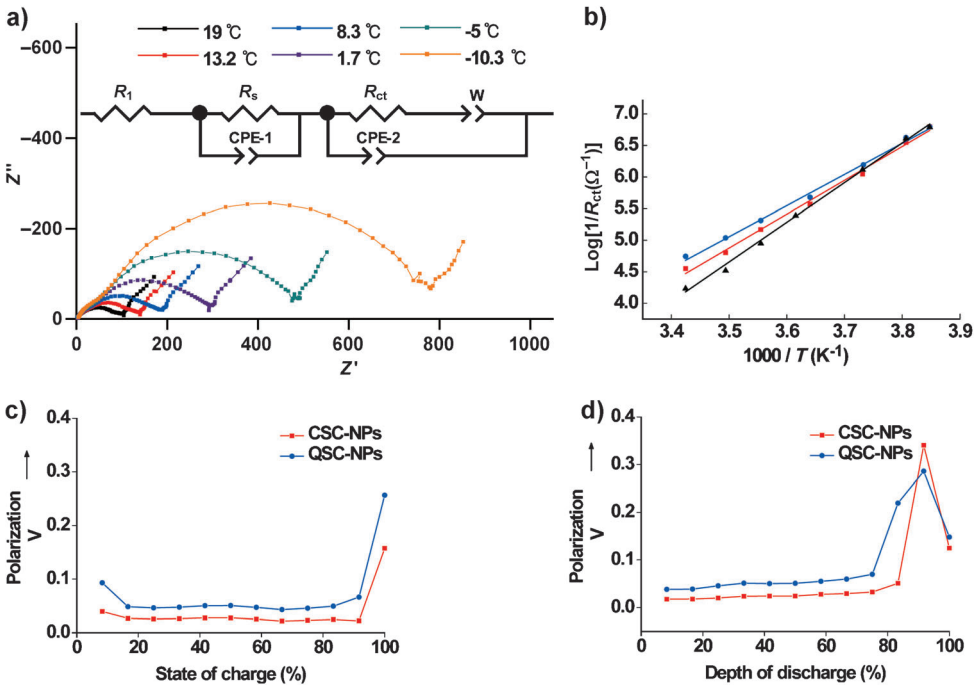

Figure 4. Electrochemical analysis. a) Nyquist plot showing electochemical impedance (*Z*) spectroscopy (EIS) data for the CSC-NPs at different temperatures. Inset of a) shows proposed equivalent circuit comprising of resistors (*R*), constant phase elements (CPE) and a Warburg element(W) .b) Arrhenius plots of the charge-transfer reaction for CSC-NPs (red square), QSC-NPs (blue circle), and PC-MPs (black triangle). Red line: $E_a = 0.46$eV, $R = 0.99$; blue line: $E_a = 0.43$eV, $R = 0.99$; black line: $E_a = 0.54$eV, $R = 0.99$. Temperature versus $1/R_{ct}$ plot was fitted from electrochemical test data (EIS; (a) and Figure S8). c, d) A plot of polarizations, which are calculated from galvanostatic intermittent titration technique (GITT) curves in Figure S9, applying a 1 C intermittent current, during charge (c) and discharge (d). QSC-NPs (blue circle) showed higher polarization than CSC-NPs (red square). E_a = activation energy, R_{ct} = charge-transfer resistance, R_s = surface resistance, R1 = solution resistance.

NPs against specific current. QSC-NPs showed much higher overpotential and ohmic resistance throughout the entire voltage profile (Figure 4c and d). Given the similar the particle size, BET, and XRD patterns of CSC-NPs and QSC-NPs as well as the slightly higher activation energy of CSC-NPs, if the rate performance of CSC-NPs and QSC-NPs electrodes were controlled by the lithium-ion diffusion in a single-crystal particle or the charge-transfer reaction on a particle surface, the polarization of CSC-NPs would be larger than that of QSC-NPs when the specific current of electrode is applied. This conflicting result is attributed to the electric-circuit configuration in the nanoparticle clusters and directly demonstrates the effect of carbon coating on single-crystal particles in nanoclusters. If all the active particles were connected electrically in parallel, the electrochemical performance of this electrode would show similar characteristics to those of single-particle electrodes.[13] Figure 1b shows a schematic view of the nanoparticle clusters. Suppose that the outer primary particles are connected with the conducting agent but the inner particles are not, as is believed to be the case for QSC-NPs: These single-crystal particles composing the clusters, can be considered as being arranged in an electrical series circuit and ionical parallel circuit because the neighboring particles and boundary interfaces provide resistance to the passage of electrons, whereas the grain boundary and particle surface can help lithium-ion diffusion. These factors decrease the specific current of the electrode to that of a few particles. Hence, the uncoated QSC-NPs experience a serious overpotential despite sharing similar characteristics with CSC-NPs and PC-MPs, which showed higher capacity retention for high rate cycle compared to QSC-NPs. Moreover the carbon-coating layer had an effect on the cycleability at elevated temperature (Figure S10). Inspite of having such a large surface area, the CSC-NPs exhibited 84 mA h g^{-1} of discharge capacity at 1 C and 100 mA h g^{-1} at 20 C after 200 cycles at 50 °C, thus indicating that the carbon layer minimizes the Mn dissolution effectively.

We have demonstrated that $LiMn_2O_4$ nanoclusters consisting of carbon-coated primary particles having a size of 20 nm size are suitable for use as a cathode material for ultrafast lithium-ion batteries. By using this material, we overcame the low-electrode-density problem of nanosized active materials while maintaining excellent rate capability. The performance is attributed to: 1) fast electrochemical reaction owing to the nanosize effect; 2) fast ion pathways to reach primary particles, such as grain boundary and particle surface; and 3) high electron conductivity in secondary particles as a result of the carbon coating of the constituent primary nanoparticles.

These efforts are an attempt to connect every single-crystal nanoparticle electrically and ionically in parallel, and we believe that these concepts offer a direct path to improving the rate capability of lithium-ion batteries without decreasing the electrode density.

Experimental Section

Materials: The nanosized $LiMn_2O_4$ particles were synthesized as follows: Manganese acetate (3.45 g) was dissolved in distilled water (30 mL). Lithium hydroxide (1.11 g) and hydrogen peroxide (1.2 mL) were dissolved in distilled water (30 mL). The two solutions were mixed with methanol (100 mL) and stirred for 20 min. The resulting slurry was poured into a Teflon-lined autoclave, and the hydrothermal reaction was carried out at 110 °C for 12 h. After the reaction was complete, the resulting solid products were filtered and washed several times with distilled water and ethanol. 13-micrometer-sized $LiMn_2O_4$ particles were synthesized by a conventional high-temper-

ature solid-state reaction. The spinel oxides were fired with stoichiometric amounts of Li_2CO_3 and MnO_2 at 780 °C for 16 h in air at a heating rate of 5 °C min^{-1}.

Carbon coating: 20 nm-sized $LiMn_2O_4$ particles (3 g) was dispersed in distilled water and ethanol (1:3 v/v; 20 mL), and the sucrose solution (0.5 g sucrose/10 mL distilled water) was added. This solution was dispersed by ultrasonication for 10 min and then concentrated to dryness. Finally, the dried powder was fired at 600 °C for 10 min and cooled quickly to room temperature with cooling rate of 10 °C min^{-1}.

Electrochemical measurements: Pouch-type half cells (cathode electrode area: 2 cm × 1 cm and 0.5 cm × 0.5 cm, lithium counter electrode : 2.5 cm × 1.5 cm and 1 cm × 1 cm) were assembled for the battery test and electrochemical test (EIS), respectively. The detailed method is described in the Supporting Information.

Received: May 9, 2012
Published online: August 2, 2012

Keywords: cathode · conducting materials · electrochemistry · lithium-ion battery · nanoparticles

[1] a) M. Yoshio, S. Inoue, M. Hyakutake, G. Piao, H. Nakamura, *J. Power Sources* **1991**, *34*, 147 – 152; b) R. J. Gummow, A. de Kock, M. M. Thackeray, *Solid State Ionics* **1994**, *69*, 59 – 67; c) P. G. Bruce, B. Scrosati, J. M. Tarascon, *Angew. Chem.* **2008**, *120*, 2972 – 2989; *Angew. Chem. Int. Ed.* **2008**, *47*, 2930 – 2946; d) Y. Xia, Y. Zhou, M. Yoshio, *J. Electrochem. Soc.* **1997**, *144*, 2593 – 2600.

[2] H.-K. Song, K. T. Lee, M. G. Kim, L. F. Nazar, *Adv. Funct. Mater.* **2010**, *20*, 3818 – 3834.

[3] a) Y. Lee, M. G. Kim, J. Cho, *Nano Lett.* **2008**, *8*, 957 – 961; b) N. Li, C. J. Patrissi, G. Che, C. R. Martin, *J. Electrochem. Soc.* **2000**, *147*, 2044 – 2049; c) A. S. Aricò, P. Bruce, B. Scrosati, J.-M. Tarascon, W. van Schalkwijk, *Nat. Mater.* **2005**, *4*, 366 – 377; d) Y. Wang, G. Cao, *Adv. Mater.* **2008**, *20*, 2251 – 2269.

[4] a) Y. Yang, C. Xie, R. Ruffo, H. Peng, D. K. Kim, Y. Cui, *Nano Lett.* **2009**, *9*, 4109 – 4114; b) E. Hosono, T. Kudo, I. Honma, H. Matsuda, H. Zhou, *Nano Lett.* **2009**, *9*, 1045 – 1051; c) K. M. Shaju, P. G. Bruce, *Chem. Mater.* **2008**, *20*, 5557 – 5562; d) Y. Zhang, H.-C. Shin, J. Dong, M. Liu, *Solid State Ionics* **2004**, *171*, 25 – 31; e) J. Luo, L. Cheng, Y. Xia, *Electrochem. Commun.* **2007**, *9*, 1404 – 1409; f) H. Yue, X. Huang, D. Lv, Y. Yang, *Electrochim. Acta* **2009**, *54*, 5363 – 5367; g) S. H. Ye, J. K. Bo, C. Z. Li, J. S. Cao, Q. L. Sun, Y. L. Wang, *Electrochim. Acta* **2010**, *55*, 2972 – 2977; h) S.-C. Park, Y.-S. Han, Y.-S. Kang, P. S. Lee, S. Ahn, H.-M. Lee, J.-Y. Lee, *J. Electrochem. Soc.* **2001**, *148*, A680 – A686; i) X. Hao, O. Gourdon, B. J. Liddle, B. M. Bartlett, *J. Mater. Chem.* **2012**, *22*, 1578 – 1591; j) B. J. Liddle, S. M. Collins, B. M. Bartlett, *Energy Environ. Sci.* **2010**, *3*, 1339 – 1346.

[5] a) J. Cho, *J. Mater. Chem.* **2008**, *18*, 2257 – 2261; b) S. Lee, S. Jeong, J. Cho, *ChemSusChem* **2010**, *3*, 1260 – 1263.

[6] O. K. Park, Y. Cho, S. Lee, H. Yoo, H.-K. Song, J. Cho, *Energy Environ. Sci.* **2011**, *4*, 1621 – 1633.

[7] a) Y.-Y. Liang, S.-J. Bao, B.-L. He, W.-J. Zhou, H.-L. Lia, *J. Electrochem. Soc.* **2005**, *152*, A2030 – A2034; b) M. Okubo, Y. Mizuno, H. Yamada, J. Kim, E. Hosono, H. Zhou, T. Kudo, I. Honma, *ACS Nano* **2010**, *4*, 741 – 752.

[8] J. Qian, M. Zhou, Y. Cao, X. Ai, H. Yang, *J. Phys. Chem. C* **2010**, *114*, 3477 – 3482.

[9] a) Y. J. Lee, H. Yi, W. J. Kim, K. Kang, D. S. Yun, M. S. Strano, G. Ceder, A. M. Belcher, *Science* **2009**, *324*, 1051 – 1055; b) B. Kang, G. Ceder, *Nature* **2009**, *458*, 190 – 193; c) H.-W. Lee, P. Muralidharan, R. Ruffo, C. M. Mari, Y. Cui, D. K. Kim, *Nano Lett.* **2010**, *10*, 3852 – 3856; d) H. Zhang, X. Yu, P. V. Braun, *Nat. Nanotechnol.* **2011**, *6*, 277 – 281.

[10] US Defense Logistics Agency, Battery Performance Characteristics, http://www.mpoweruk.com/performance.htm.

[11] a) J. C. Fisher, *J. Appl. Phys.* **1951**, *22*, 74 – 77; b) H. C. Yu, A. Van Der Ven, K. Thornton, *Appl. Phys. Lett.* **2008**, *93*, 091908; c) R. E. Hoffman, D. Turnbull, *J. Appl. Phys.* **1951**, *22*, 634 – 639; d) N. Balke, S. Jesse, A. N. Morozovska, E. Eliseev, D. W. Chung, Y. Kim, *Nat. Nanotechnol.* **2010**, *5*, 749 – 754.

[12] a) J. Jamnik, J. Maier, *Phys. Chem. Chem. Phys.* **2003**, *5*, 5215 – 5220; b) N. Sata, K. Eberman, K. Eberl, J. Maier, *Nature* **2000**, *408*, 946 – 949; c) J. Maier, *Nat. Mater.* **2005**, *4*, 805 – 815.

[13] a) K. Dokko, N. Nakata, K. Kanamura, *J. Power Sources* **2009**, *189*, 783 – 785; b) K. Dokko, N. Nakata, Y. Suzuki, K. Kanamura, *J. Phys. Chem. C* **2010**, *114*, 8646 – 8650.

